MATH8803 - Final Project: A Survey on the Best Methods for EEG/MEG Motor Imagery Functional Brain Network Representation

Matthew Chen

April 2024

1 Introduction

Inspired by C.J. Stam's 2012 paper *Go with the flow: Use of a directed phase lag index (dPLI) to characterize phase relations in a large-scale model of brain dynamics*, this report is on evaluating different functional connectivity measures from Electroencephalography (EEG) data to determine which measure's modeling directly reflects real-world data [32]. Note that these experimental methods can be transferred to Magnetoencephalography (MEG) data because both EEG and MEG data are often modeled as stochastic and periodic time series. The evaluation of various functional connectivity measures has been studied by many in the past three decades; however, these evaluations are primarily based on simulated EEG data and rely on certain coupling dynamics assumptions [39, 18]. To formally define the task performed, as stated in [39], we want to measure functional connectivity, the statistical dependence among measured time series. The time series analyzed in this project are EEG signals and information exchange in the brain has been demonstrated to be encoded in their statistical dependencies [14, 6]. A typical EEG dataset consists of around 17 to 22 channels, laid out in the internationally recognized 10-20 system, which represents electrodes that measure electric potential changes on the scalp of the brain. Under the assumption that these channels approximate the postsynaptic potentials of groups of neurons directly below their corresponding electrode, each channel represents a different cortical region of the brain. Besides evaluating functional connectivity measures, we also evaluate the direction in which information flows by using certain functional connectivity measures that not only indicate statistical dependence between time series, and the direction of dependence, as suggested in [32]. The lack of analysis on using functional connectivity measures for the direction of information flow in literature justifies this direction.

1.1 Dataset

The EEG signals used in our experiments were provided by the Mother of all BCI Benchmarks (MOABB), a Python library hosting several freely available EEG datasets [2]. We use the widely studied `BNCI2014_001` dataset from MOABB, dataset IIa from BCI competition 4 hosted in 2012 [35]. A short description of the dataset is that it consists of EEG data from 9 subjects, where time series are labeled with a different class based on four different motor imagery tasks: the imagination of movement of the left-hand, right-hand, both feet and tongue. For each subject, data was recorded over 2 days in two sessions, where each session comprised 6 runs, and each run comprised 48 trials, where 12 trials were for each of the four classes, yielding 288 trials per session. To reduce potential variance in brain network architectures, we only analyzed the first subject. In total, there are 576 trials and there are 22 channels for each trial and 1000 sampled data points sampled at 250 Hz over 4 seconds. The stimulus presented to the subject was present one second before recording. In most subsequent analyses, we only analyzed the first 1-2 seconds of the data since previous experiments demonstrate the importance of temporal encoding in spikes [25]. Furthermore, the data was pre-processed to remove noise and normalize the signals. An interesting avenue of investigation is determining if dynamics are different in the different motor imagery tasks.

2 Models

2.1 Functional Connectivity Measures and the Directed Phase Lag Index

C.J. Stam originally proposed the phase lag index (PLI) in 2007 [33], which measures the phase synchronization of two-time series, specifically applied to EEG/MEG signals, and is not sensitive to volume conditions or common reference effects. Essentially, the metric performs spectral analysis such that the current phase state of the signal is found and a measure of the correlation between two-time series is outputted. More formally, given time series 1 and 2, we can calculate the current phase of the two-time series Φ_1 and Φ_2, and $\Phi_{1,2}$ is the difference between the two:

$$|\Phi_{1,2}| = |n\Phi_1 - m\Phi_2| < const$$

where n, m are constants. Φ_1 and Φ_2 are calculated using the analytical signal concept and the Hilbert Transform. Suppose $s_1(t)$ represents the time series of signal 1 and $\hat{s}_1(t)$ is the Hilbert transform of the signal. Then the analytical signal $\Psi_1(t)$ is a complex function:

$$\Psi_1(t) = s_1(t) + i\hat{s}_i(t) = A(t)e^{i\phi_i(t)}$$

Moreover, the Hilbert transform is calculated as:

$$\hat{s}_i(t) = \pi^{-1}\text{P.V.}\int_{-\infty}^{\infty}\frac{s_1(\tau)}{t-\tau}d\tau$$

where P.V. is the Cauchy principle value. Finally, the phase of signal 1 at time t is computed as:

$$\Phi_1(t) = \arctan(\frac{\hat{s_1}(t)}{s_1(t)})$$

Then PLI represents the norm of the phase difference distribution if it were put into a vector:

$$PLI = |\langle sign(\Phi_t)\rangle|$$

The directed phase lag index (dPLI) is very similar to the phase lag index; however, it gives more information in indicating the direction of causality between the two signals [32]. Instead of taking the absolute value of the vector, the dPLI between signals 1 and 2 is defined as:

$$dPLI_{1,2} = \frac{1}{N}\sum_{t=1}^{N} H(\Phi_t)$$

where H is the Heaviside step function. Like PLI, dPLI is a value between 0 and 1, and when $0.5 < dPLI_{1,2} \leq 1$ it means that series 1 is consistently phase leading compared to 2 and it $0 \leq dPLI_{1,2} < 0.5$ that means that 1 is consistently lagging compared to 2. If $dPLI_{1,2} = 0.5$ or around it, it typically means neither leading or lagging on average. Note that one can reconstruct the PLI from the dPLI:

$$PLI = 2|0.5 - dPLI|$$

A criticism of these two methods is that [8] mentioned that these metrics are not sensitive to coupling relationships with small time lags. In other words, when these metrics indicate a coupling relationship, that means one can be confident it is a true relationship; however, this also means that it might filter out more subtle true relationships. In statistical terms, this means minimizing Type 1 error but increasing Type 2 error. A more frequently used method is the weighted Phase Lag Index (wPLI) by [38] that takes into probabilistic weightings of the phase distribution into account and will also be considered in our experiments in conjunction with dPLI.

2.2 Phase Slope Index

Another functional connectivity metric we will experiment with is the Phase Slope Index (PSI), proposed by Nolte et. al in 2008 [24] and has previously been used in EEG/MEG analysis [4]. The metric has several machine-learning and biological applications and has been empirically shown to provide fewer false positive results compared to the more popular Granger causality [23]. To calculate the PSI, first, the dataset is split into K segments of duration T, and the cross-spectral density is estimated:

$$S_{ij}(f) = \frac{1}{K} \sum_{k} z_i(f,k) z_j^*(f,k)$$

where $z_i(f,k)$ is the Fourier transform of the Hanning-windowed. Next, coherence is calculated as:

$$C_{ij}(f) = \frac{S_{ij}(f)}{\sqrt{S_{ii} S_{jj}(f)}}$$

Finally, the PSI is calculated as:

$$\tilde{\Psi}_{ij} = \Im(\sum_{f \in F} C_{ij}^*(f) C_{ij}(f + \delta f))$$

where $\Im$ represents taking the imaginary part and $\delta f = 1/T$ is the frequency resolution. F is the set of frequencies over which the slope is summed.

2.3 EEG Source Interaction Dynamics

Certain functional connectivity measures have been demonstrated to perform better under certain coupling dynamic assumptions relative to other measures and also depend on what measures of dependency should be emphasized [31]. Define $x_i(t)$ as the signal of node i at time t, where $i \in \{1, \ldots, n\}$ with n the number of nodes and $\epsilon_i(t)$ as the noise at node i at time t, represented as an uncorrelated standard normal distributed random variable. In the case of EEG signal analysis, nodes are electrodes. Two ways to integrate a value for measuring dependency between the time series involves autoregressive coefficients or a pairwise connection strength matrix [18, 39]. Details about the most common coupling dynamic assumptions (models) are listed below.

2.3.1 Jansen-Rit Neural Mass Model (NMM)

Moran et. al., 2013 [22] had introduced a modified Jansen-Rit Neural Mass Model which could simulate EEG data which was also used as the NMM in [39]. Furthermore, the Jansen-Rit Neural Mass model is an extension of the model proposed by Lopes Da Silva and van Rotterdam in the 1970s [37, 10, 11]. In the original dPLI paper [32], C.J. Stam used an augmented model from Da Silva and van Rotterdam described in [34, 27]. Specifically, the one used in [22] is a convolution-based neural mass model for EEG data that generates EEG data at the millisecond timescale. It's a biologically plausible model that considered three subpopulations within cortical columns: spiny stellate cells in granular layer IV, pyramidal cells, and inhibitory interneurons, which are in granular layers II, III, V, and VI. The main connection dynamics are between pyramidal subpopulations and spiny stellate subpopulations. The precise mathematical definition of this model is extensive and will not be explicitly defined here, but can be found in the original paper [22] and also in section 1.1 of the Supplementary material of [39]. A quick gist of the model is that it generates 13 neural states, 5 of which are current potentials $i_0 - i_5$ and 7 which are membrane potentials of the 3 subpopulations $v_1 - v_7$. A more comprehensive history of these NMMs can be found in [29].

2.4 Coupled Linear Systems

The first way to model linear interactions between two-time series from two sources is by using a bivariate linear autoregressive model, which was used in [18]:

$$\begin{bmatrix} x_1(t) \\ x_2(t) \end{bmatrix} = \sum_{p=1}^{P} \begin{bmatrix} a_{11}(p) & a_{12}(p) \\ a_{21}(p) & a_{22}(p) \end{bmatrix} \begin{bmatrix} x_1(t-p) \\ x_2(t-p) \end{bmatrix} + \begin{bmatrix} \varepsilon_1(t) \\ \varepsilon_2(t) \end{bmatrix}$$

Here, P represents the total amount of look-back on the time series and $p \in \{1, \ldots, P\}$. If we denote time series 1 as i and time series 2 as j, then $a_{ij}(p)$ represents the linear autoregressive coefficients or correlation matrix between the two signals at lookback p. Similarly, in [39], the linear system is produced by:

$$\dot{x}_i(t) = \sum_{p=1}^{P} \sum_{j=1}^{n} C_{ij} x_j(t-p) + \epsilon_i(t)$$

where C_{ij} represents the coupling strength between node i and j with lookback p. We use the former set of equations to generate simulated EEG signals where the off-diagonal entry $a_{12}(p) = 0$ but $a_{21}(p) = 0.5$. The other coefficients where set to 0, which meant that there was a unidirectional time-delayed influence of $x_1(t)$ on $x_2(t)$, like [18].

2.5 Coupled Non-Linear Systems

These systems are used to measure and emulate the chaos in the recorded time series dynamics under certain parameter values and initial conditions, which are not specified here but are assumed to be the default values that would generate these chaotic solutions.

2.5.1 Lorenz System

A classic system of 3 ordinary differential equations, the Lorenz system is defined as:

$$\frac{dx}{dt} = \sigma(y - x)$$

$$\frac{dy}{dt} = x(\rho - z) - y$$

$$\frac{dz}{dt} = xy - \beta z$$

In generating coupled signals, such as in [18], all potential pairwise combinations of the signals are considered. In other words, analysis of pairwise signals between (x, y), (x, z), (y, z) represent different non-linear coupling dynamics.

2.5.2 Rössler System

Each node is based on the Rössler attractor, which is an attractor for the Rössler system, which is a set of three non-linear ordinary differential equations:

$$\frac{dx}{dt} = -y - z$$

$$\frac{dy}{dt} = x + ay$$

$$\frac{dz}{dt} = b + z(x - c)$$

[18] had generated signals like how they generated pairwise coupled signals for the Lorenz system. However, [39] defined each node as having its own Rössler system:

$$\frac{dx}{dt} = -ay_i(t) - z_i(t) + \epsilon_i(t) + \sum_p \sum_j C_{ij}(x_j(t-p) - x_i(t))$$

$$\frac{dy}{dt} = -ax_i(t) - dy_i(t)$$

$$\frac{dz}{dt} = b + z_i(t)(x_i(t) - c)$$

using previously defined notation. Here x_i would represent the signal generated by node i and y_i and z_i are the unobserved variables contributing to the dynamics.

2.5.3 Hénon System

Pairwise coupled signals are generated by a Hénon map, a two-dimensional discrete-time dynamical system described as:

$$x_{n+1} = 1 - ax_n^2$$

$$y_{n+1} = bx_n$$

[18] generates pairwise signals using these equations. On the other hand, [39] assumes each node a Hénon map:

$$x_i(t) = 1.4 - \sum_j C_{ij}x_i(t)x_j(t) - (1 - \sum_j C_{ij})x_i^2(t) + bx_i(t-1) + \epsilon_i(t+1)$$

Something interesting to note is that, although Hénon maps have frequently been used to model the chaotic systems of neural signals, recently [17] have experimentally demonstrated that classical Hénon maps are poor models for describing the chaos of the system by comparing the simulated data with neurophysiological data. A major goal of this report is to extend [17] analyses to the other non-linear systems using neurophysiological data from [35].

2.6 Measuring the similarity of time series dynamics using the Shannon entropy-statistical complexity plane

2.6.1 The Bandt-Pompe (BP) Technique

The BP technique estimates the underlying probability distribution function of a time series by encoding the time series as a sequence of symbols [3]. A brief explanation of the technique is as follows, however specific details can be found in the original paper by Bandt and Pompe [3]:

1. Suppose we are given a time series $x(t)$ where $t \in \{1, \ldots, M\}$ where M is the number of measurements. We want to identify ordinal structures in fixed-size windows of the series by considering all possible permutations of the values. This can then be used to generate a probability distribution of ordinal patterns. Suppose this time series is $x(t) = \{10, 13, 15, 12, 20, 18, 25\}$ where $M = 7$. Though in practice $M \gg D!$.

2. Their two parameters for this method D, the embedding dimension, and τ, the time delay. Once determined, the time series is partitioned into $n = M - (D-1)\tau$ overlapping segments. Each window has D observations and these observations are separated by τ. In most literature $D = 3$, which gives us $D! = 6$ permutations that we can encode [19, 17, 18]. The time delay τ is usually equal to 1, as Bandt and Pompe originally only assumed $\tau = 1$, and analysis with $\tau > 1$ was introduced by subsequent authors. Assume $D = 3$ and $\tau = 1$ and denote the 6 symbolic encoding permutations as the letters A, B, C, D, E, F.

3. Assign each window with its permutation label. In our example, each window is 3 observations, and considering the first window it would be $(10, 13, 25)$. Because in this window $x_0 \leq x_1 \leq x_2$, the inequality defines the permutation corresponding to the letter A. The next window would be $(13, 15, 12)$, and here $x_2 \leq x_0 \leq x_1$ would also correspond to another letter (say B). The probability distribution is simply the frequency of these symbols amongst all n partitions. Figure 1 in the appendices created by [19] shows a more visual explanation. They used this symbolic transform method to create another functional connectivity method: weighted Symbolic Mutual Information (wSMI), which has been empirically shown to index consciousness [19].

4. Using this PDF, various information-theoretic quantities can be calculated, as these values characterize the time series and its dynamics.

2.7 The Shannon Entropy-Statistical Complexity Plane

Statistical complexity is a metric used to measure the differences in dynamical systems that originated from L'opez-Ruit et. al [20]. Like the approach in [17], we use the specific Martin-Rosso-Plastino (MPR) statistical complexity [21]. This is given by:

$$C_{Jensen-Shannon}[P] = \mathcal{Q}_J[P, P_e] \cdot H[P] \tag{1}$$

where H is the normalized Shannon entropy defined by $H[P] = \frac{S[P]}{S_{\max}}$ with $S_{\max} = S[P_e] = \log_2 N$ and $0 \leq H \leq 1$. $\mathcal{Q}$ is known as the disequilibrium and is a function of the Jensen-Shannon divergence:

$$\mathcal{Q}_J[P, P_e] = Q_o \mathcal{J}[P, P_e] \tag{2}$$

where Q_o is a normalization constant so that $0 \leq \mathcal{Q}_j \leq 1$ and the Jensen-Shannon Divergence is defined as:

$$\mathcal{J}[P, P_e] = H[\frac{P + P_e}{2}] - \frac{H[P]}{2} - \frac{H[P_e]}{2} \tag{3}$$

The Jensen-Shannon divergence, similar to KL divergence, is a metric for comparing probability distributions, often used for analyzing distributions of random variables represented as symbols. P represents the probability distribution being analyzed and P_e represents the uniform distribution. A detailed/annotated figure of the Complexity-Entropy plane can be found in the Appendix in Figure 2. In the figure, the maximum and minimum complexity possible given the Shannon Entropy is plotted, with correlated noise in between the bounds. Stochastic behaviors of the dynamic systems usually have lower complexity than correlated noise while chaotic behaviors usually have maximum complexity. By plotting the calculated complexity and entropy of this plane, one can analyze how these systems exhibit similarities or differences in their relationships of complexity and entropy. Similar systems are expected to have similar relationships between the two quantities.

2.7.1 Fisher Information

Besides calculating complexity with respect to entropy, we also compare Fisher information with respect to entropy identical to [17]. Compared to Shannon's entropy, Fisher information is sensitive to local changes and is defined as:

$$F[f] = \int \frac{|\vec{\nabla} f(x)|^2}{f(x)} dx$$

where f is a continuous PDF, which means the Fisher information is highly sensitive to the gradient of the PDF. We numerically calculate the Fisher information using the method described in [26].

3 Methods

3.1 Simulating NMMs and Lorenz, Rössler, and Hénon Systems

3.1.1 Lorenz, Rössler, and Hénon Systems

The three systems were implemented in Python using a Forward Euler method and each variable and their pairwise time series solutions were averaged and also analyzed. For each system, $10,000$ simulated points were generated and windows of length 250 were aggregated. For the Hénon map the initial state was $(x_0, y_0) = (0, 0)$ with $a = 1.4, b = 0.3$ and both the two-dimensional and single-channel decomposition were analyzed with time steps of $\Delta t = 0.1$. The Rössler system used initial values of $(x_0, y_0, z_0) = (0.1, 0.1, 0.1)$ with $a = 0.2, b = 0.2, c = 5.7$ and timesteps of $\Delta t = 0.1$. The Lorenz system had initial conditions $(x_0, y_0, z_0) = (0, 1, 1.05)$ with parameters $\sigma = 10, \beta = 8/3, \rho = 28$ with timestep $\Delta T = 0.01$.

3.1.2 Neural Mass Models

There exist several Python libraries that already implement popular Neural Mass Models including `Neurolib` and `Pyrates` [7, 15]. We decided to use `Neurolib` to create a network of Jansen-Rit NMMs to reproduce the work found in [32] as this is the most similar pre-implemented model we could find compared to the NMM used in [32]. This is a system of 78 NMMs representing the 78 AAL regions and each NMM is coupled using additive coupling of their firing rates (though other simulated coupling methods could be explored and the specific coupling used in [32] is described in [13]). We approximate this network with 80 NMMs, their measured functional connectivity, and their fiber length matrix, found from the Human Connectome Project for ease of implementation [36]. Moreover, to further simplify, we use the Wilson-Cohan model, which only models excitatory and inhibitory neurons in a neuronal mass, but is much more computationally efficient to simulate. We fix each mass to the default parameters but perform a parameter search on the global coupling coefficient and the coupling delay. The excitatory output of the neurons is then used as the EEG signal and the average dPLI to the other masses for each mass was calculated.

3.2 Producing the Complexity-Entropy (and related) planes

After acquiring the data, all of the subsequent analyses are performed in Python. Given the complexity of implementing the Bandt-Pompe approach, luckily, there exists a library `ordpy` recently publicized by Pessa and Ribeiro [26] that performs this method for us. A particularly useful feature of this library is that their function `complexity_entropy`, which returns the complexity and entropy value of a given time series, works for multi-dimensional time series. We can leverage this given that there are multiple channels and each of these channels records different parts of the brain at each timestep. The choice of parameters for the Bandt-Pompe process is complex as noted in [17] and to capture interesting information, we decided to set parameters to maximize the amount of variation in permutation entropy and statistical complexity as we hypothesize that more variation captures more information. Specifically, we considered windows where $D = 5$ and the time delay $\tau = 3$ even though smaller windows often capture more interesting information and a smaller D captures more short-lived interactions because these parameters showed the most variance. Additionally, due to how much variance is in this larger distribution, even stochastic systems may be diagnosed as chaotic under these analysis parameters. This is due to the increased precision by having a greater number of symbols. There are two ways we can model these signals as a chaotic system. The first, as previously mentioned, is to consider the entirety of the brain as a chaotic system in which the permutation of the values of each channel encodes a specific state of the brain. The second is to assume that each channel, i.e. the neuronal assembly directly below the electrode is an individual chaotic system and each channel's system influences one another, which was assumed in [39]. We explore both cases by presenting statistics of the ordinal distribution analyzed under these different views.

3.3 Measuring chaos via Lyapunov Exponents

Furthermore, another simple metric for measuring the chaos in a system is through Lyapunov exponents [17]. Essentially, Lyapunov exponents are a characteristic of a system that measures how much it diverges when given two slightly varying initial conditions. In other words, it is defined as:

$$\|f^{(N)}(x_0 + \delta_0) - f^{(N)}(x_0)\| = |\delta_0|e^{\lambda n}$$

where x_0 represents the initial state of the system, $x_0 + \delta_0$ represents the same initial state with a small δ_0 perturbation, N represents the number of time steps after the initial condition and λ is the Lyapunov exponent. Although there are closed-form solutions for calculating Lyapunov exponents from known systems, we are interested in calculating these exponents from time series data. Again, luckily, Christopher Schölzel has publicized the Python library `nolds`, which stands for NOnLinear measures for Dynamical Systems, which implements several Lyapunov exponent calculation methods [30]. Specifically, we use `nolds.lyap_r`, which estimates the largest Lyapunov exponent from a one-dimensional time series using the RANSAC algorithm, a method proposed by Rosenstein et. al [28]. We consider each channel from each trial individually. While `nolds` is great for one-dimensional time-series, it fails to consider multi-dimensional time series and thus will not help us analyze under the perspective that the whole brain network is a dynamic system. Therefore, we implemented a custom Lyapunov exponent estimation method for multivariate time series inspired by code from [12]. We considered the vector of initial states of each channel as representing the initial state of the whole system and considered the closeness of initial states as the Euclidean distance between the two in different trials separated by their motor imagery label. We used the heuristic of comparing initial states that had a distance less than the mean of all non-zero distances between pairs and analyzed the relationship between the distribution of the logarithm of the Euclidean distance between the two-time series as the systems evolved. We plot both the maximum and average Lyapunov exponents estimated at each time step for each motor imagery label. An interesting thing to note is that, although all Lyapunov exponents calculated were positive, it should still be taken with a grain of salt whether the system is chaotic as [5] has demonstrated that stochastic models are also able to produce the outputs of chaotic systems. In our opinion, we hypothesize there might exist a better metric for measuring chaos than the Lyapunov exponent as the line between chaotic and stochastic systems is blurry and potentially there might exist a numerical quantity of chaotic systems that approaches infinity in stochastic systems that could distinguish the two.

3.4 Functional Connectivity Measures and Analysis

Similar to the previous methods, we luckily already have a package that implements the functional connectivity measures and helps with visualization. The package `mne`, is a popular open-source Python package for exploring, visualizing, and analyzing neuropsychological data [16]. We leverage its pre-existing implementations of functional connectivity measures and pre-processing methods in our experiments. We also use another library called `NiLearn` for visualization [9].

4 Results

Note that all figures mentioned are presented in the Appendix due to page limits.

4.1 The choice between $D = 3$ and $D = 5$

Although many works set $D = 3$, we investigated $D = 5$ since we analyzed up to 1 second which enables more windows to examine despite the large window size. Using ordpy's `ordinal_distribution` a plot of the Ordinal PDF of trial 0 (which is a tongue trial) during the first 400 ms of recording is shown when $D = 3$ and a corresponding Ordinal PDF for when $D = 5$ is shown in Figures 3 and 4 respectively. In both cases, $\tau = 3$ was used.

4.2 Statistical Complexity C and Fisher Information F w.r.t Entropy H

Figure 5 shows the MPR-Complexity with respect to Shannon Entropy H if we were to analyze each channel as a chaotic system. Each dot represents a single time series of a channel from a specific trial. Figure 6 is combining all the figures from Figure 5 onto the same graph. Figure 7 is plotted under the case where we consider the whole brain network as the system, i.e. each dot represents a trial, and we consider all channels' time series in conjunction. Figure 8 is the Fisher Information vs Entropy plot under the multi-channel analysis. We considered three different time windows to analyze to determine whether information is lost as time from the visual stimulation elapsed.

4.3 Linear Coupling

We also simulated the bivariate auto-regression linear coupling relationship using the previously mentioned parameters. We set the maximum time to $T = 10000$ and had a window size of 250 with a lookback period of $P = 5$. We also checked if averaging the signals would show different dynamics and included them in our analysis as well. The complexity-entropy plot is shown in Figure 9.

4.4 Nonlinear and Chaotic Dynamical Systems

When simulating the three dynamical systems, we set the maximum time to $T = 10000$ integration steps and analyzed windows of size 250 (assuming each window is independent of the previous window). To cover more varied dynamics, and potentially coupling relationships, we performed pairwise averaging of the system's variables (depending on how many variables the system had) and plotted them. Figures 10, 11, 12, and 13 show the complexity entropy plots for the 2D Hénon, 1D Hénon, Rössler and Lorenz systems respectively.

4.5 Lyapunov Exponents

4.5.1 Individual Channel Analysis

Using the algorithm from [30], we calculate the maximum Lyapunov exponents for the time series considering different time windows. Note that these were not separated by motor imagery. The average of each channel is shown in Table 14. Again the embedding dimension was set to 5 and the delay was set to 3.

4.5.2 Multi-Channel Analysis

Here we calculate the distribution of Lyapunov exponents of time series separated into their different imaging categories. We don't explicitly calculate the Lyapunov exponents, but they are the coefficients of the line fit to the linear part of the graphs at the beginning since the distance of the initial conditions is log-scaled. We can't consider the entire graph since the values of the time series are bounded. Moreover, in Figure 15 we consider the maximum and the average of each distribution. The linear parts of the graphs spike very early, at around between $k = 0$ to $k = 10$.

4.6 Directed Functional Connectivity

We analyzed the first 300 time steps consistent with our previous analyses and split the trials between motor imagery stimuli. We analyze between the frequency range of 8hz to 30hz as these are the most common frequency ranges in motor imagery analysis [1].

4.6.1 Directed Phase Lag Index (dPLI)

Note that the dPLI adjacency matrices are asymmetric because dPLI is inherently a bidirectional value (despite indicating direction), which is shown in Figure 16. Graphs for each motor imagery are found in Figures 17a, 17b, 17c, and 17d.

4.6.2 Weighted Phase Lag Index (wPLI)

Unlike the $dPLI$, the $wPLI$ *is* bidirectional, hence we only need the lower triangle of the matrix. Only the top 20 connections (highest weight) are shown in Figure 19.

4.6.3 Phase Slope Index (PSI)

Similar to the last two sections, a similar analysis was done in Figures 20 and 21.

4.7 Recreating Results from [32]

As mentioned before, for ease of implementation, we used the connectivity matrix and fiber length matrix from the Human Connectome project and applied it to a network of Wilson-Cowan neural mass models in `neurolib`. Specifically, we first performed a parameter search on global coupling coefficients $k_{gl} = \{3, 5, 6, 7, 10\}$ and coupling delay of $Signal_V = \{27.5, 30, 32.5, 35, 37.5\}$ over 1 second durations where $\Delta t = 0.1ms$. We also downsampled the signals using `scipy.signal.resample` to simulate 250 Hz and then calculated the dPLI for the signals within the α and β bands. Figure 22 shows parameters found that showed significant coupling relationships based on dPLI, i.e the dPLI values deviated from 0.5. Each AAL region was averaged in the computation over all of its dPLI values with the other regions and the averages are plotted. We decided to use the parameters $k_{gl} = 10$ and $Signal_V = 32.5$ and then ran the model for 20 seconds with the same timestep. We again downsampled and plotted the complexity-entropy plot in Figure 23.

5 Discussion + Conclusion

We originally hypothesized that the properties of the dynamics would be different in different motor imagery tasks; however, based 5, 6, 7 it seems that the properties of the dynamics generally remain consistent. Furthermore, under these analysis parameters, it appears the properties are more Hënon-ic compared to the Lorenz, Rössler, and bivariate linear autoregression in Figures 10, 11, 12, 13 and 9. However, a cause for concern is that the Figure 9 should be close to the lower curve as suggested by 2 since we intentionally simulated a stochastic system. The relationship between complexity and entropy does become stochastic when $D = 3$ rather than $D = 5$, which suggests that the large support for our symbol encoding might be too precise (similar to the concept of overfitting) where even stochastic systems could become chaotic under extremely complex analysis. There is also a philosophical question of whether the random number generator provided by Python is truly random or simply using a chaotic pseudorandom number generator to generate its values. In terms of directly measuring chaos, it seems that as longer time stretches are analyzed, the system becomes more and more chaotic based on Figure 7. Finally, the Lyapunov exponents from 14 support that belief because they, on average, increase as longer windows are analyzed. For the functional connectivity analysis, the dPLI and wSMI seem to agree on the most important connections among the channels' signals. However, the PSI seems to show clearer distinctions between the motor imagery category types. In simulating the data under a network of 80 neural masses each represented using a Wilson-Cohan model in an attempt to recreate the results from [32], the inconsistency in the results after varying model parameters demonstrates major downfalls of dPLI. It seems that the NMMs and parameters they used [32] were specifically tailored to present the effectiveness of the metric but failed to capture coupling relationships in other models. The code used to perform these experiments can be found on Github. There is also an addendum at the end of this report explaining future work and learnings from these experiments.

6 Appendix

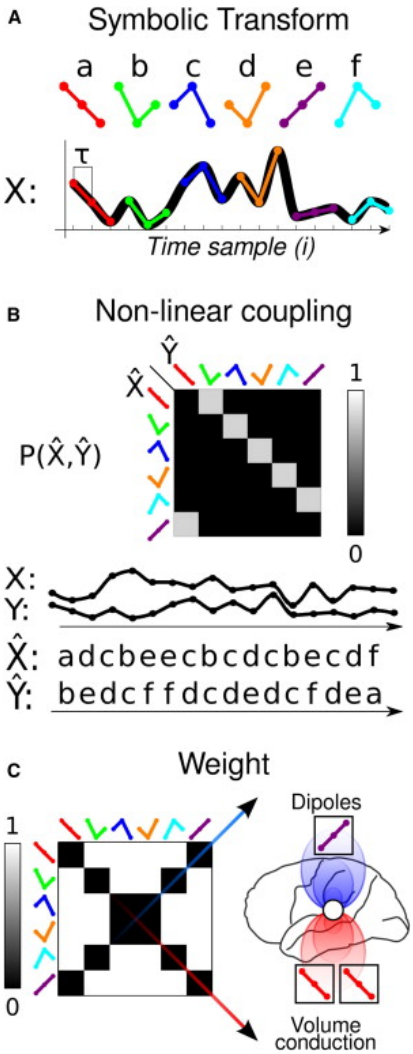

Figure 1: Figure from [19]

7 Addendum

In terms of future work, there is still a lot to be analyzed from this dataset and potential extensions by comparing it with other datasets. This dataset was simply chosen out of convenience and ease of implementation due to being heavily studied in the literature. Some future experiments that can be done in decreasing order of priority/potential novelty include but are not limited to:

1. **Parameter Optimization** - Determining programmatically how to fit existing models to the data. Both `neurolib` and `Pyrates` offer solutions for parameter fitting via evolutionary algorithms, and `Scipy` offers its own through the differential evolution strategy. In doing so, these could make our results more precise and convincing because all of the previously mentioned parameters were chosen arbitrarily or are defaults.

2. **Further Data-Processing Methods** - We only used the first subject in our experiments; however there would be more than 100 million data points if we included the other subjects. We could also perform averaging of similar trials/channels to reduce the amount of processed data and reduce the variance/stochasticity of the signals. Furthermore, we could analyze performing deep learning to featurize these signals such as a model like Time2Vec or manually engineering a specific kernel (such as extracting their power spectra) for these signals to gain a new perspective on them.

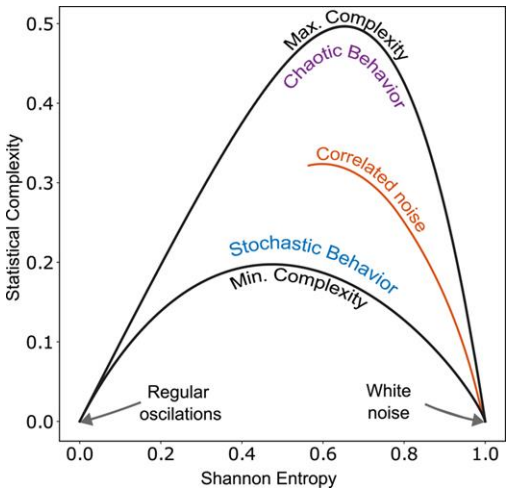

Figure 2: Figure from [17]

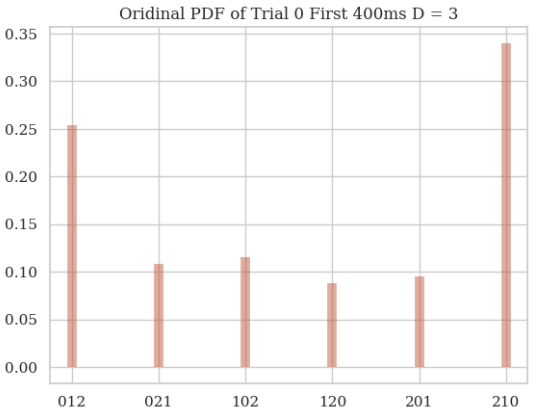

Figure 3: Trial 0 Ordinal PDF, $D = 3$

3. **Combining multiple functional connectivity measures** - Something lacking in functional connectivity analysis in literature is the presence of using multiple functional connectivity measures in tandem to achieve a more comprehensive view of the brain network. Most literature primarily focuses on single functional connectivity measures. Potentially, by combining several and performing statistical analysis on them one could discover both linear and nonlinear coupling relationships in one experiment.

4. **Modifying the Parameters in the Bandt-Pompe Process** - As mentioned previously, using a large support for the symbolic encoding of the signals generally characterized all signals, simulated and real, as chaotic. It seems that reducing the size of the embedding window in addition to changing the analysis window could uncover more novel insights about the data. Furthermore `ordpy` has a lot to offer that we did not exploit here.

5. **Other Measures of Chaos** - We could incorporate other measures of chaos, such as the Hurst exponent, which are already implemented in `nolds`, to further compare dynamics and solidify our conclusions.

6. **Better Exploration of NMM simulation libraries** - Seeing that we do not want to reinvent the wheel, it would be beneficial to explore more of `neurolib` and `Pyrates` and determine if we could make a better/more biologically plausible NMM network from their implementations.

Also, some things I learned and things I learned do NOT work include:

1. **Parameter Fitting of Chaotic Dynamical Systems** - I attempted to originally fit the Hénon system to EEG data using `Scipy's` optimization functions. However, that turned out to be impossible due to

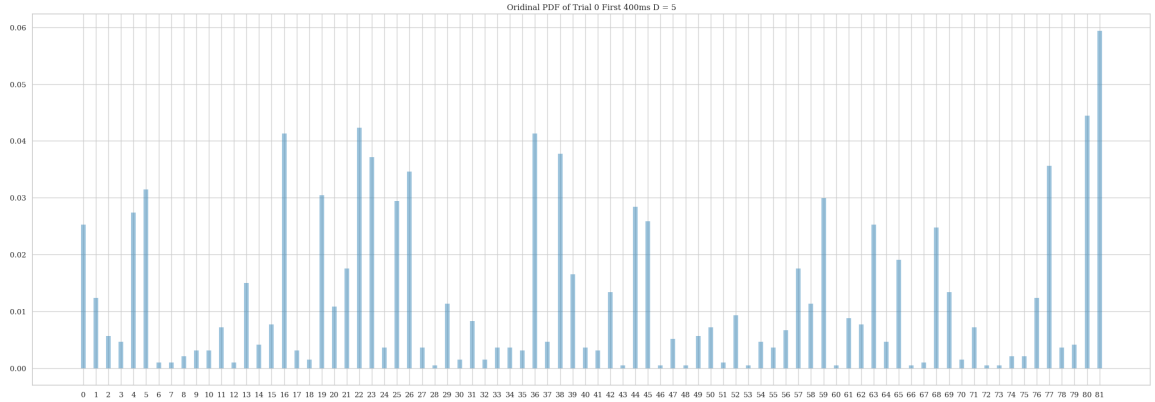

Figure 4: Trial 0 Ordinal PDF, $D = 5$

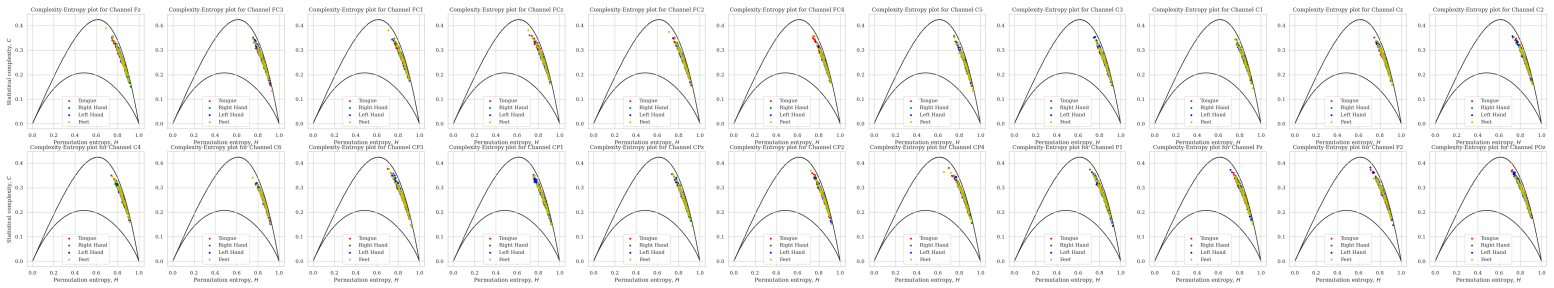

Figure 5: Complexity-Entropy Plot for each channel for Subject #0

the explosion in the size of the search space and the overflow errors that occurred due to how chaotic the system was. Small changes in a few parameters made certain numerical computations excessive, which probably owes itself to the chaos of the system and thus I currently do not know if there are numerical methods for fitting that circumvent this problem. As I mentioned before, differential evolution is another algorithm that could work since it doesn't perform integration/calculate derivatives.

2. **Renyi Complexity vs Entropy** - Renyi complexity is calculated in a similar way to MPR complexity, and I realized that comparing it against permutation entropy did not provide any significant interesting results.

3. **Simulating the Jansen-Rit NMM is difficult** - Originally, before implementing the Wilson Cowan NMM network, I tried to mirror the model proposed in [32] using `neurolib`. However, I realized that the lack of documentation, several bugs, and inefficient computations made it practically impossible to implement. `neurolib` uses `jitcdde` and `numba` as backends for solving differential equations and these libraries are extremely slow when the number of equations grows linearly. Since the Jansen-Rit model is an extremely complicated system, and there were 80 NMMs, it was impossible to run simulations of the network of Jansen-Rit models due to the enormous amount of time it took to complete even an integration step.

4. **EEG Signal Preprocessing** - Luckily the BNCI dataset already filtered for frequencies between 8 and 32 Hz, which correspond to the Alpha and Beta bands. However, I still learned what band-pass filters were and how they were related to the frequency domain/Fourier transforms.

5. **3D Visualization of Functional Connectivity** - I originally wanted to create a 3D plot one could interact with in a Jupyter notebook using the MNE library, but the difficulty of integrating a graphical application inside a headless Linux machine made it infeasible, which is why I opted to use `NiLearn`. However, based on the examples from MNE, it seems that one could plot the functional connectivity of the EEG signals in sensor space on top of a 3D model of a person's head.

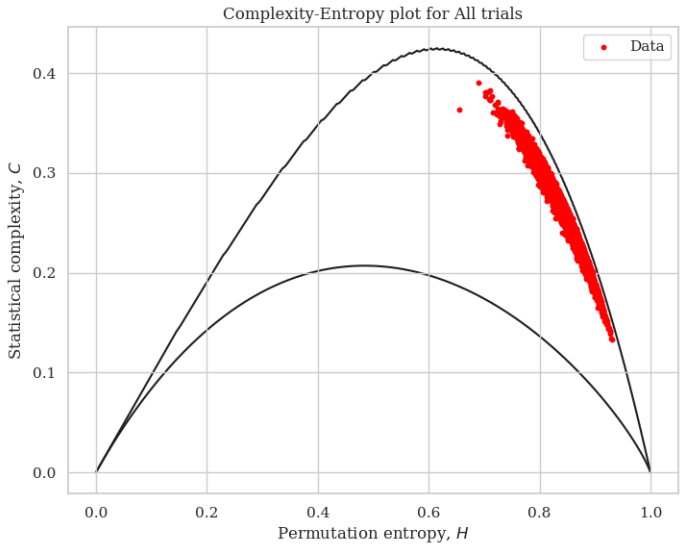

Figure 6: All trials Complexity-Entropy Plot (Each dot represents a channel time series)

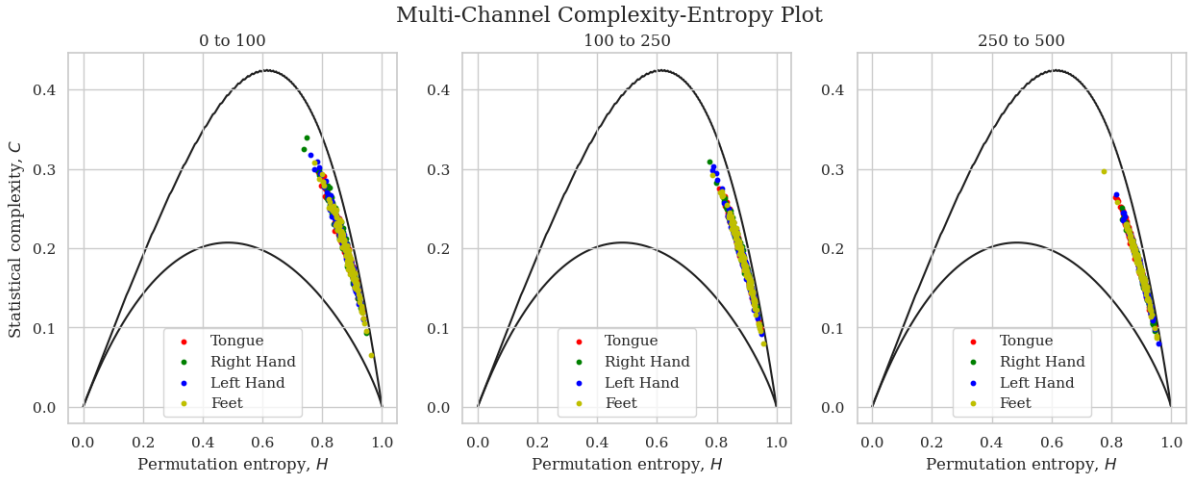

Figure 7: Subplot titles represent index windows analyzed

References

[1] Sajjad Afrakhteh and Mohammad Reza Mosavi. Chapter 2 - applying an efficient evolutionary algorithm for eeg signal feature selection and classification in decision-based systems. In Amr Mohamed, editor, *Energy Efficiency of Medical Devices and Healthcare Applications*, pages 25–52. Academic Press, 2020.

[2] Bruno Aristimunha, Igor Carrara, Pierre Guetschel, Sara Sedlar, Pedro Rodrigues, Jan Sosulski, Divyesh Narayanan, Erik Bjareholt, Barthelemy Quentin, Robin Tibor Schirrmeister, Emmanuel Kalunga, Ludovic Darmet, Cattan Gregoire, Ali Abdul Hussain, Ramiro Gatti, Vladislav Goncharenko, Jordy Thielen, Thomas Moreau, Yannick Roy, Vinay Jayaram, Alexandre Barachant, and Sylvain Chevallier. Mother of all BCI Benchmarks, 2023.

[3] Christoph Bandt and Bernd Pompe. Permutation entropy: A natural complexity measure for time series. *Phys. Rev. Lett.*, 88:174102, Apr 2002.

[4] Alessio Basti, Vittorio Pizzella, Federico Chella, Gian Luca Romani, Guido Nolte, and Laura Marzetti. Disclosing large-scale directed functional connections in meg with the multivariate phase slope index. *NeuroImage*, 175:161–175, 2018.

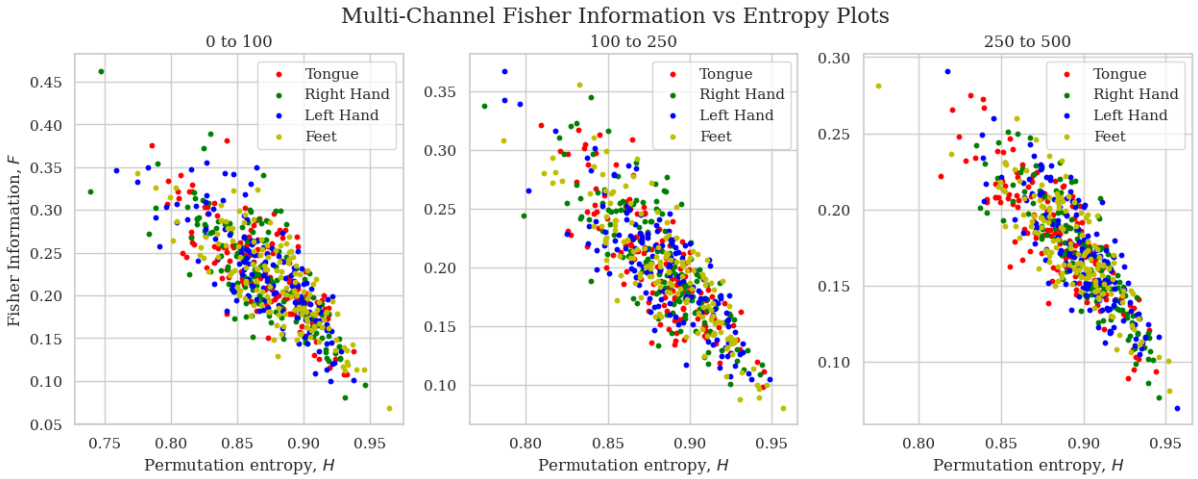

Figure 8: Subplot titles represent index windows analyzed

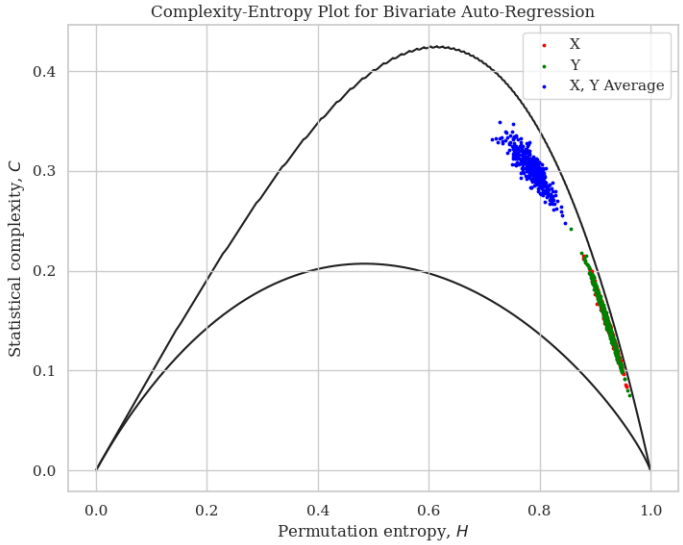

Figure 9: Complexity-Entropy Plot for Bi-Variate Linear Coupling

[5] B. Biswal and C. Dasgupta. Stochastic neural network model for spontaneous bursting in hippocampal slices. *Physical Review E*, 66(5), November 2002.

[6] Ed Bullmore and Olaf Sporns. The economy of brain network organization. *Nature reviews neuroscience*, 13(5):336–349, 2012.

[7] Caglar Cakan, Nikola Jajcay, and Klaus Obermayer. neurolib: A simulation framework for whole-brain neural mass modeling. *Cognitive Computation*, Oct 2021.

[8] Michael X Cohen. Effects of time lag and frequency matching on phase-based connectivity. *Journal of Neuroscience Methods*, 250:137–146, July 2015.

[9] Nilearn contributors, Ahmad Chamma, Aina Frau-Pascual, Alex Rothberg, Alexandre Abadie, Alexandre Abraham, Alexandre Gramfort, Alexandre Savio, Alexandre Cionca, Alexis Thual, Alisha Kodibagkar, Amadeus Kanaan, Ana Luisa Pinho, Andrés Hoyos Idrobo, Anne-Sophie Kieslinger, Ariel Rokem, Arthur Mensch, Aswin Vijayan, Audrey Duran, Ben Cipollini, Bertrand Thirion, Binh Nguyen, Caglar Cakan, Chris Gorgolewski, Chris Markiewicz, Christian Horea, Christian Gerloff, Christina Roßmanith, Colin Reininger, Connor Lane, Czarina Sy, Céline Delettre, Dan Gale, Daniel Gomez, Danilo Bzdok, David G Ellis, Demian Wassermann, Derek Pisner, Dimitri Papadopoulos Orfanos, Elizabeth DuPre, Elvis Dohmatob,

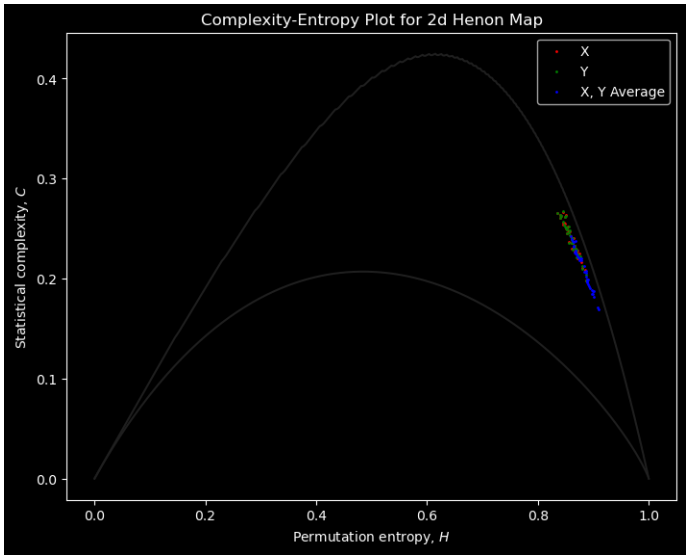

Figure 10: Complexity-Entropy Plot for 2D Henon Map

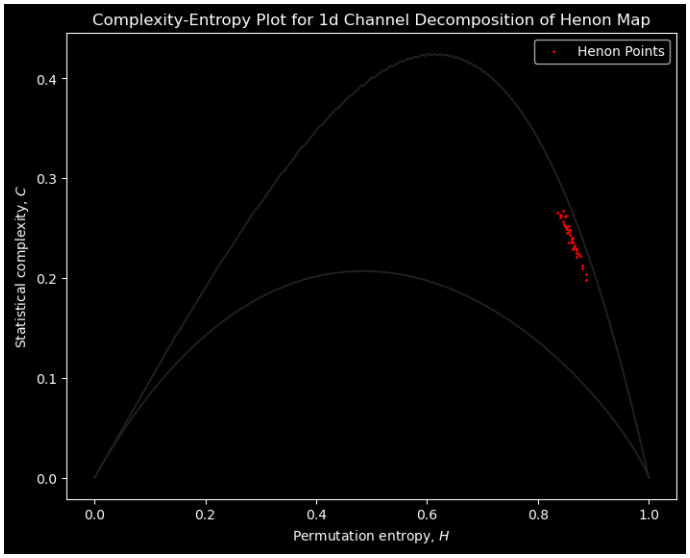

Figure 11: Complexity-Entropy Plot for 1D Decomposition of Henon Map

Eric Larson, Evan Edmond, Fabian Pedregosa, Florent Pollet, Franz Liem, François Paugam, Gael Varoquaux, Gilles de Hollander, Greg Kiar, Greydon Gilmore, Guillaume Lemaitre, Hao-Ting Wang, Himanshu Aggarwal, Ian Abenes, Jake Vogel, Jan Margeta, Jaques Grobler, Jason Gors, Javier Rasero, Jean Kossaifi, Jean-Rémi King, Jelle Roelof Dalenberg, Jeremy Lefort-Besnard, Jerome Dockes, Jerome-Alexis Chevalier, Johannes Wiesner, Jon Haitz Legarreta Gorrono, Jona Sassenhagen, Jordi Huguet, Joshua Teves, Julia Huntenburg, Julio A Peraza, Kamalakar Reddy Daddy, Kevin Sitek, Koen Helwegen, Konrad Wagstyl, Konstantin Shmelkov, Kshitij Chawla, Kun CHEN, Leonard Sasse, Loic Estève, Loic Tetrel, Luz Paz, Manon Pietrantoni, Martin Perez-Guevara, Martin Wegrzyn, Mathias Goncalves, Mathieu Dugré, Matthias Ekman, Matthieu Joulot, Maximilian Cosmo Sitter, Mehdi Rahim, Mia Zwally, Michael Eickenberg, Michael Hanke, Michael Notter, Michael Waskom, Michelle Wang, Mohammad Torabi, Moritz Boos, Myeong Seop Song, Natasha Clarke, Neelay Shah, Nicolas Gensollen, Nikhil Krish, Oliver Warrington, Oscar Esteban, Patrick Sadil, Paul Bogdan, Paul Reiners, Paula Sanz-Leon, Peer Herholz, Philippe Gervais, Pierre Bellec, Pierre Glaser, Pierre-Olivier Quirion, Pradeep Reddy Raamana, Rahul Brito, Raphael Meudec, Robert Luke, Robert Williamson, Roberto Guidotti, Ronald Phlypo, Ryan Hammonds, Rémi Gau, Sachin Patalasingh, Sage Hahn, Salma Bougacha, Sam Buck Johnson, Sami Jawhar, Simon Steinkamp, Sourav Singh, Steven Meisler, Suramya Pokharel, Sylvain Lan, Sylvain Takerkart, Tamer Gezici, Tarun Samanta, Taylor

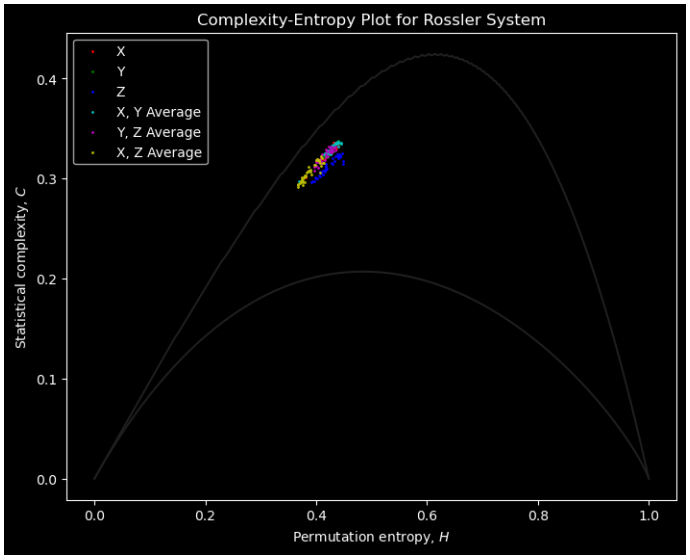

Figure 12: Complexity-Entropy Plot of Rössler System

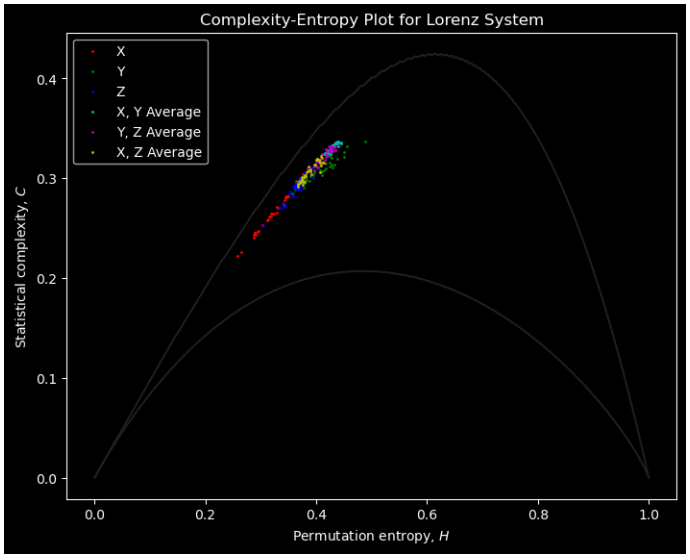

Figure 13: Complexity-Entropy Plot of Lorenz System

Salo, Thomas Bazeille, Tom Vanasse, Vasco Diogo, Vincent Michel, Virgile Fritsch, Yaroslav Halchenko, Yasmin Mzayek, Zvi Baratz, and Óscar Nájera. nilearn, April 2024.

[10] FH Lopes Da Silva, A Hoeks, H Smits, and LH Zetterberg. Model of brain rhythmic activity. the alpha-rhythm of the thalamus. *Kybernetik*, 15(1):27–37, 1974.

[11] FH Lopes Da Silva, A Van Rotterdam, P Barts, E Van Heusden, and W Burr. Models of neuronal populations: the basic mechanisms of rhythmicity. *Progress in brain research*, 45:281–308, 1976.

[12] Abhranil Das. Calculating the lyapunov exponent of a time series (with python code), 2014.

[13] Willem de Haan, Katherine Mott, Elisabeth C. W. van Straaten, Philip Scheltens, and Cornelis J. Stam. Activity dependent degeneration explains hub vulnerability in alzheimer's disease. *PLoS Computational Biology*, 8(8):e1002582, August 2012.

[14] Karl J. Friston. Functional and effective connectivity in neuroimaging: A synthesis. *Human Brain Mapping*, 2(1–2):56–78, January 1994.

	Window Analyzed		
Channel	First 100	First 250	First 1000
Fz	0.03517496	0.05442131	0.07078728
FC3	0.03533038	0.05441394	0.07069911
FC1	0.03535783	0.05453457	0.07087332
FCz	0.0349184	0.05457023	0.07079232
FC2	0.03604976	0.05484078	0.07071474
FC4	0.03636985	0.05488332	0.07083639
C5	0.03631975	0.05511046	0.07082049
C3	0.03553935	0.05435952	0.07086788
C1	0.03603844	0.05489454	0.07121942
Cz	0.03519987	0.05476009	0.07089726
C2	0.03607272	0.05486243	0.07076262
C4	0.03661789	0.0550317	0.07067475
C6	0.03635146	0.05561067	0.07150041
CP3	0.03501571	0.05415585	0.0701516
CP1	0.03551226	0.05505894	0.07096774
CPz	0.03640859	0.0550349	0.07128839
CP2	0.03668091	0.05523475	0.0710431
CP4	0.03613862	0.05455311	0.07043317
P1	0.03536008	0.054622	0.0706847
Pz	0.03675358	0.05509541	0.0710047
P2	0.03610426	0.05520038	0.07098495
P0z	0.03756362	0.05556658	0.07186629

Figure 14: Average Lyapunov Exponents of Individual Channels

[15] Richard Gast, Daniel Rose, Christoph Salomon, Harald E. Möller, Nikolaus Weiskopf, and Thomas R. Knösche. Pyrates—a python framework for rate-based neural simulations. *PLOS ONE*, 14(12):e0225900, December 2019.

[16] Alexandre Gramfort, Martin Luessi, Eric Larson, Denis A. Engemann, Daniel Strohmeier, Christian Brodbeck, Roman Goj, Mainak Jas, Teon Brooks, Lauri Parkkonen, and Matti S. Hämäläinen. MEG and EEG data analysis with MNE-Python. *Frontiers in Neuroscience*, 7(267):1–13, 2013.

[17] Natalí Guisande, Monserrat Pallares di Nunzio, Nataniel Martinez, Osvaldo A. Rosso, and Fernando Montani. Chaotic dynamics of the Hénon map and neuronal input–output: A comparison with neurophysiological data. *Chaos: An Interdisciplinary Journal of Nonlinear Science*, 33(4):043111, 04 2023.

[18] Laura Sophie Imperatori, Monica Betta, Luca Cecchetti, Andrés Canales-Johnson, Emiliano Ricciardi, Francesca Siclari, Pietro Pietrini, Srivas Chennu, and Giulio Bernardi. Eeg functional connectivity metrics wpli and wsmi account for distinct types of brain functional interactions. *Scientific Reports*, 9(1), June 2019.

[19] Jean-Rémi King, Jacobo D Sitt, Frédéric Faugeras, Benjamin Rohaut, Imen El Karoui, Laurent Cohen, Lionel Naccache, and Stanislas Dehaene. Information sharing in the brain indexes consciousness in noncommunicative patients. *Current biology*, 23(19):1914–1919, 2013.

[20] Ricardo Lopez-Ruiz, Hector L Mancini, and Xavier Calbet. A statistical measure of complexity. *Physics letters A*, 209(5-6):321–326, 1995.

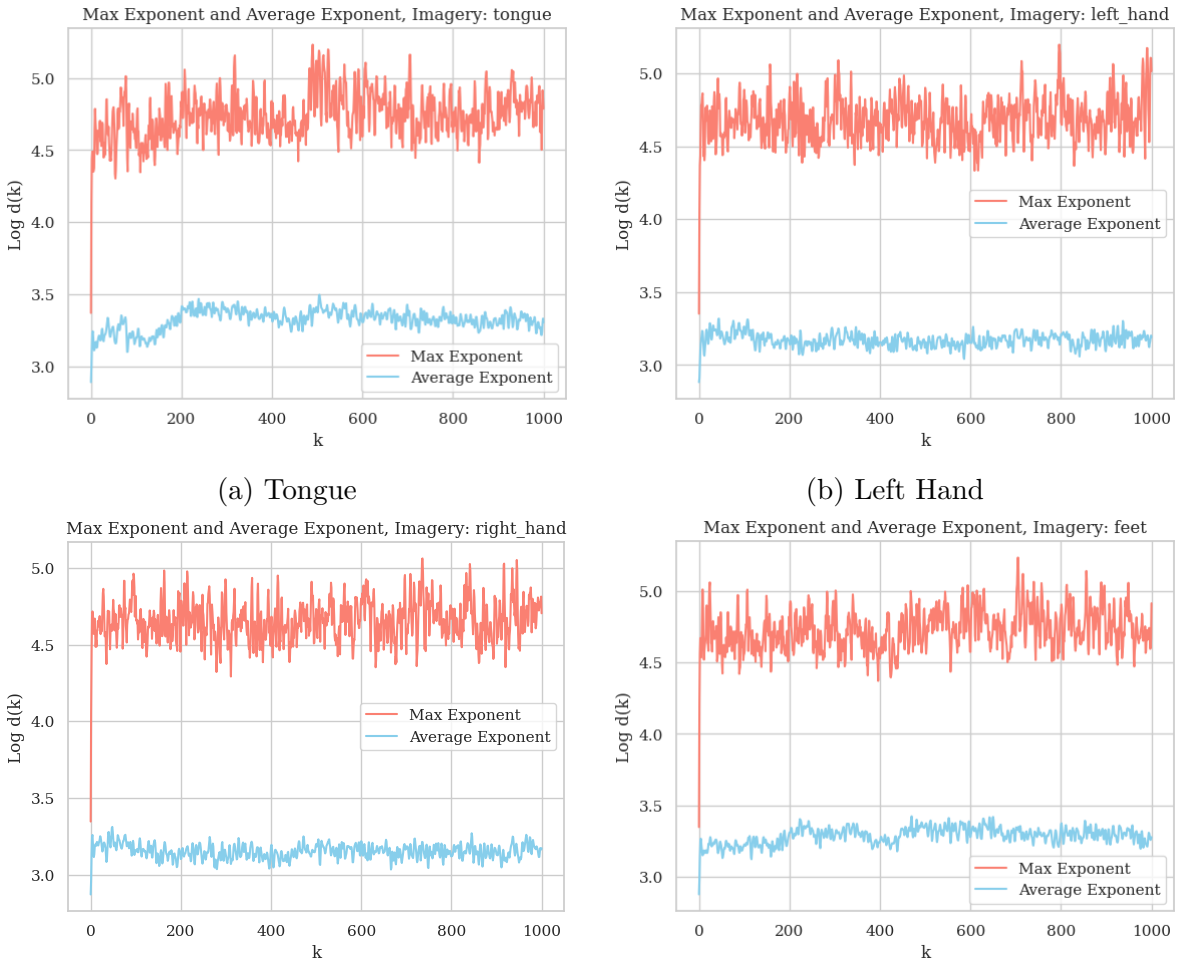

(a) Tongue

(b) Left Hand

(c) Right Hand

(d) Feet

Figure 15: Multi-Channel Lyapunov Exponent Estimation (Linear fit of the linear part of graph = λ)

[21] MT Martin, A Plastino, and Osvaldo A Rosso. Generalized statistical complexity measures: Geometrical and analytical properties. *Physica A: Statistical Mechanics and its Applications*, 369(2):439–462, 2006.

[22] Rosalyn Moran, Dimitris Pinotsis, and Karl Friston. Neural masses and fields in dynamic causal modeling. *Frontiers in Computational Neuroscience*, 7, 2013.

[23] Guido Nolte, Andreas Ziehe, Nicole Krämer, Florin Popescu, and Klaus-Robert Müller. Comparison of granger causality and phase slope index. In Isabelle Guyon, Dominik Janzing, and Bernhard Schölkopf, editors, *Proceedings of Workshop on Causality: Objectives and Assessment at NIPS 2008*, volume 6 of *Proceedings of Machine Learning Research*, pages 267–276, Whistler, Canada, 12 Dec 2010. PMLR.

[24] Guido Nolte, Andreas Ziehe, Vadim V. Nikulin, Alois Schlögl, Nicole Krämer, Tom Brismar, and Klaus-Robert Müller. Robustly estimating the flow direction of information in complex physical systems. *Physical Review Letters*, 100(23), June 2008.

[25] Stefano Panzeri, Rasmus S Petersen, Simon R Schultz, Michael Lebedev, and Mathew E Diamond. The role of spike timing in the coding of stimulus location in rat somatosensory cortex. *Neuron*, 29(3):769–777, 2001.

[26] Arthur A. B. Pessa and Haroldo V. Ribeiro. ordpy: A Python package for data analysis with permutation entropy and ordinal network methods. *Chaos: An Interdisciplinary Journal of Nonlinear Science*, 31(6):063110, 06 2021.

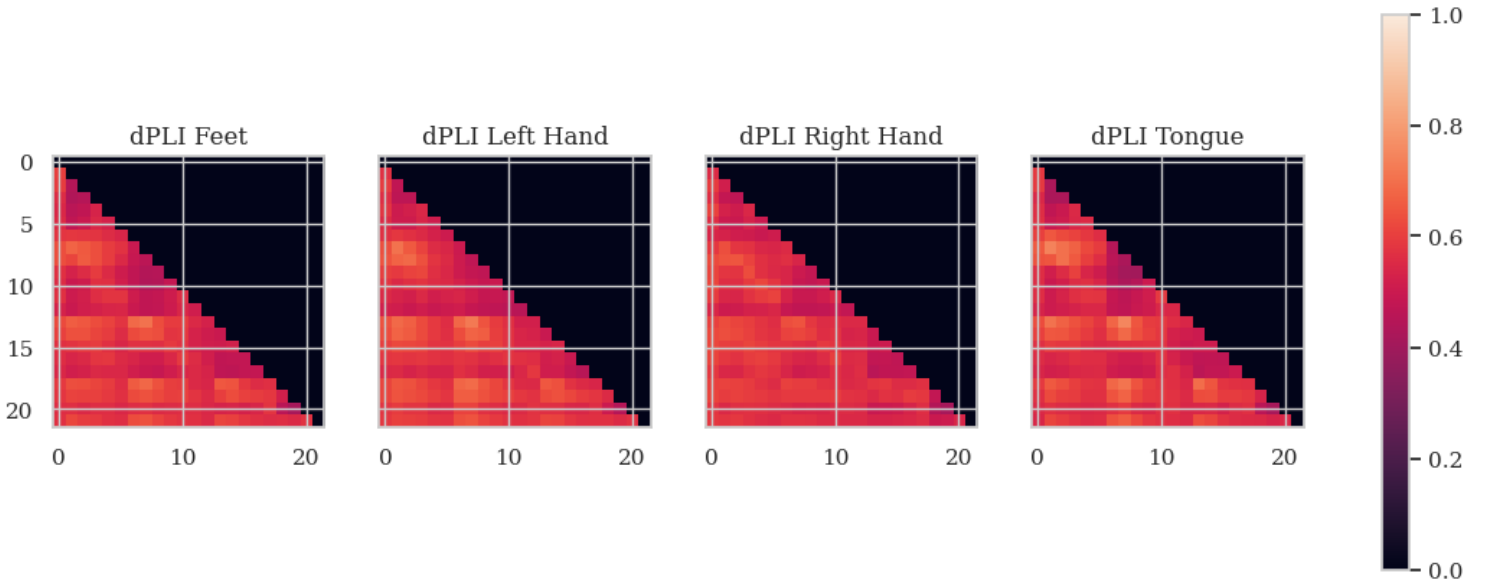

Figure 16: dPLI Pairwise Adjacency Matrices

[27] S.C. Ponten, A. Daffertshofer, A. Hillebrand, and C.J. Stam. The relationship between structural and functional connectivity: Graph theoretical analysis of an eeg neural mass model. *NeuroImage*, 52(3):985–994, 2010. Computational Models of the Brain.

[28] Michael T. Rosenstein, James J. Collins, and Carlo J. De Luca. A practical method for calculating largest lyapunov exponents from small data sets. *Physica D: Nonlinear Phenomena*, 65(1):117–134, 1993.

[29] Roser Sanchez-Todo, André M. Bastos, Edmundo Lopez-Sola, Borja Mercadal, Emiliano Santarnecchi, Earl K. Miller, Gustavo Deco, and Giulio Ruffini. A physical neural mass model framework for the analysis of oscillatory generators from laminar electrophysiological recordings. *NeuroImage*, 270:119938, 2023.

[30] Christopher Schölzel. Nonlinear measures for dynamical systems, May 2020.

[31] Stephen M Smith, Karla L Miller, Gholamreza Salimi-Khorshidi, Matthew Webster, Christian F Beckmann, Thomas E Nichols, Joseph D Ramsey, and Mark W Woolrich. Network modelling methods for fmri. *Neuroimage*, 54(2):875–891, 2011.

[32] C.J. Stam and E.C.W. van Straaten. Go with the flow: Use of a directed phase lag index (dpli) to characterize patterns of phase relations in a large-scale model of brain dynamics. *NeuroImage*, 62(3):1415–1428, 2012.

[33] Cornelis J. Stam, Guido Nolte, and Andreas Daffertshofer. Phase lag index: Assessment of functional connectivity from multi channel eeg and meg with diminished bias from common sources. *Human Brain Mapping*, 28(11):1178–1193, January 2007.

[34] Cornelis Jan Stam, Arjan Hillebrand, Huijuan Wang, and Piet Van Mieghem. Emergence of modular structure in a large-scale brain network with interactions between dynamics and connectivity. *Frontiers in Computational Neuroscience*, 4, 2010.

[35] Michael Tangermann, Klaus-Robert Müller, Ad Aertsen, Niels Birbaumer, Christoph Braun, Clemens Brunner, Robert Leeb, Carsten Mehring, Kai J. Miller, Gernot Mueller-Putz, Guido Nolte, Gert Pfurtscheller, Hubert Preissl, Gerwin Schalk, Alois Schlögl, Carmen Vidaurre, Stephan Waldert, and Benjamin Blankertz. Review of the bci competition iv. *Frontiers in Neuroscience*, 6, 2012.

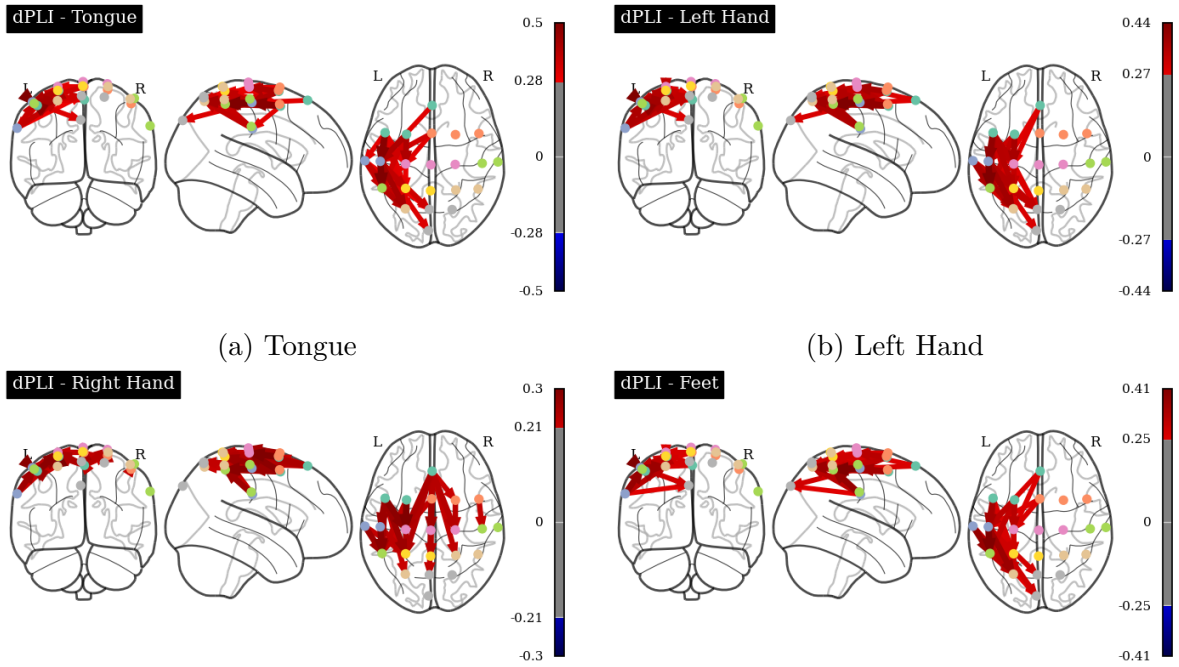

(a) Tongue

(b) Left Hand

(c) Right Hand

(d) Feet

Figure 17: Brain Connectivity Graphs using dPLI

[36] D.C. Van Essen, K. Ugurbil, E. Auerbach, D. Barch, T.E.J. Behrens, R. Bucholz, A. Chang, L. Chen, M. Corbetta, S.W. Curtiss, S. Della Penna, D. Feinberg, M.F. Glasser, N. Harel, A.C. Heath, L. Larson-Prior, D. Marcus, G. Michalareas, S. Moeller, R. Oostenveld, S.E. Petersen, F. Prior, B.L. Schlaggar, S.M. Smith, A.Z. Snyder, J. Xu, and E. Yacoub. The human connectome project: A data acquisition perspective. *NeuroImage*, 62(4):2222–2231, 2012. Connectivity.

[37] 3A van Rotterdam, FH Lopes Da Silva, J Van den Ende, MA Viergever, and AJ Hermans. A model of the spatial-temporal characteristics of the alpha rhythm. *Bulletin of mathematical biology*, 44(2):283–305, 1982.

[38] Martin Vinck, Robert Oostenveld, Marijn van Wingerden, Franscesco Battaglia, and Cyriel M.A. Pennartz. An improved index of phase-synchronization for electrophysiological data in the presence of volume-conduction, noise and sample-size bias. *NeuroImage*, 55(4):1548–1565, 2011.

[39] Huifang E. Wang, Christian G. Bénar, Pascale P. Quilichini, Karl J. Friston, Viktor K. Jirsa, and Christophe Bernard. A systematic framework for functional connectivity measures. *Frontiers in Neuroscience*, 8, 2014.

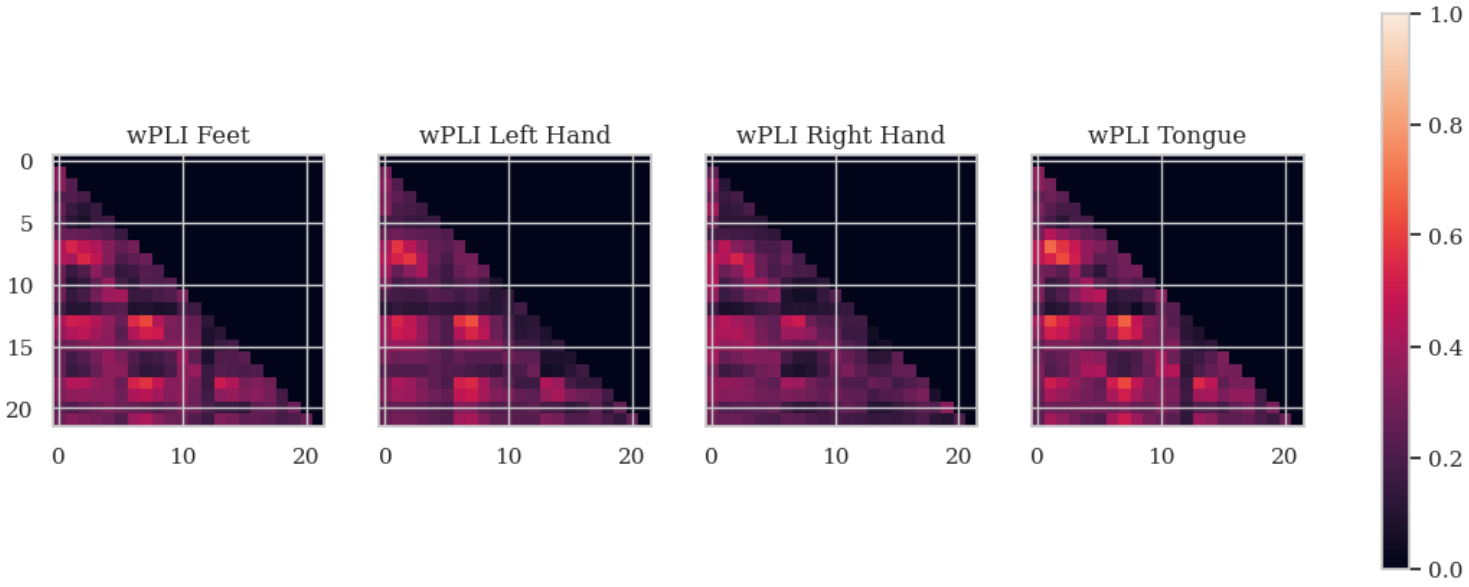

Figure 18: wPLI Pairwise Adjacency Matrices

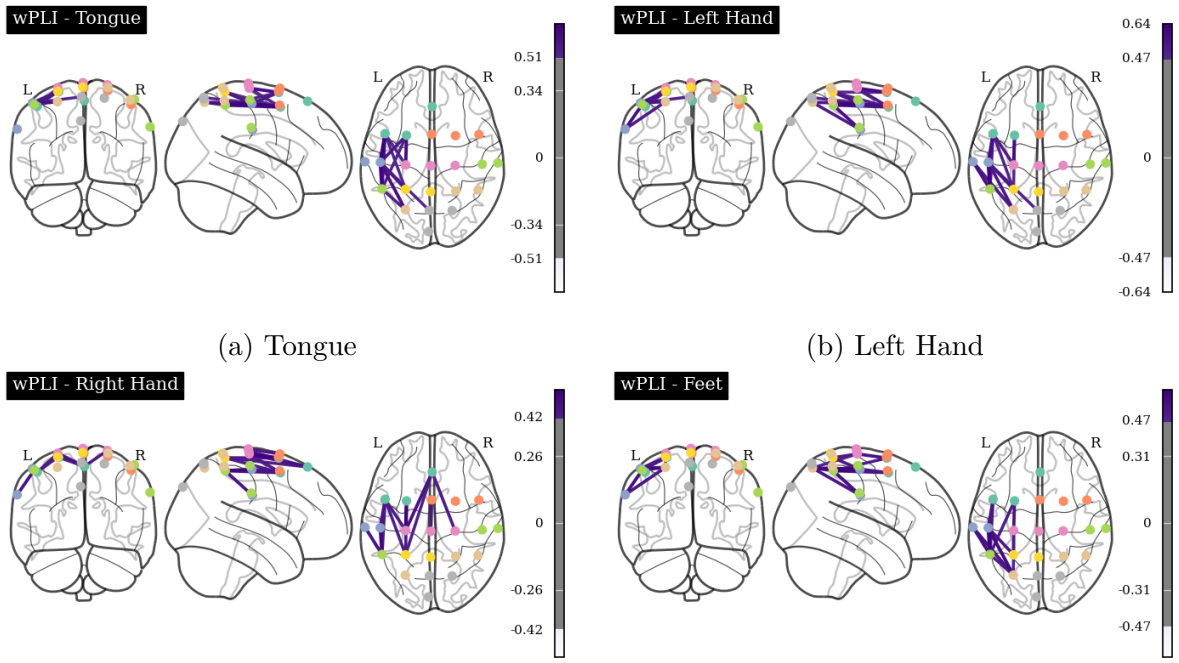

(a) Tongue

(b) Left Hand

(c) Right Hand

(d) Feet

Figure 19: Brain Connectivity Graphs using wPLI

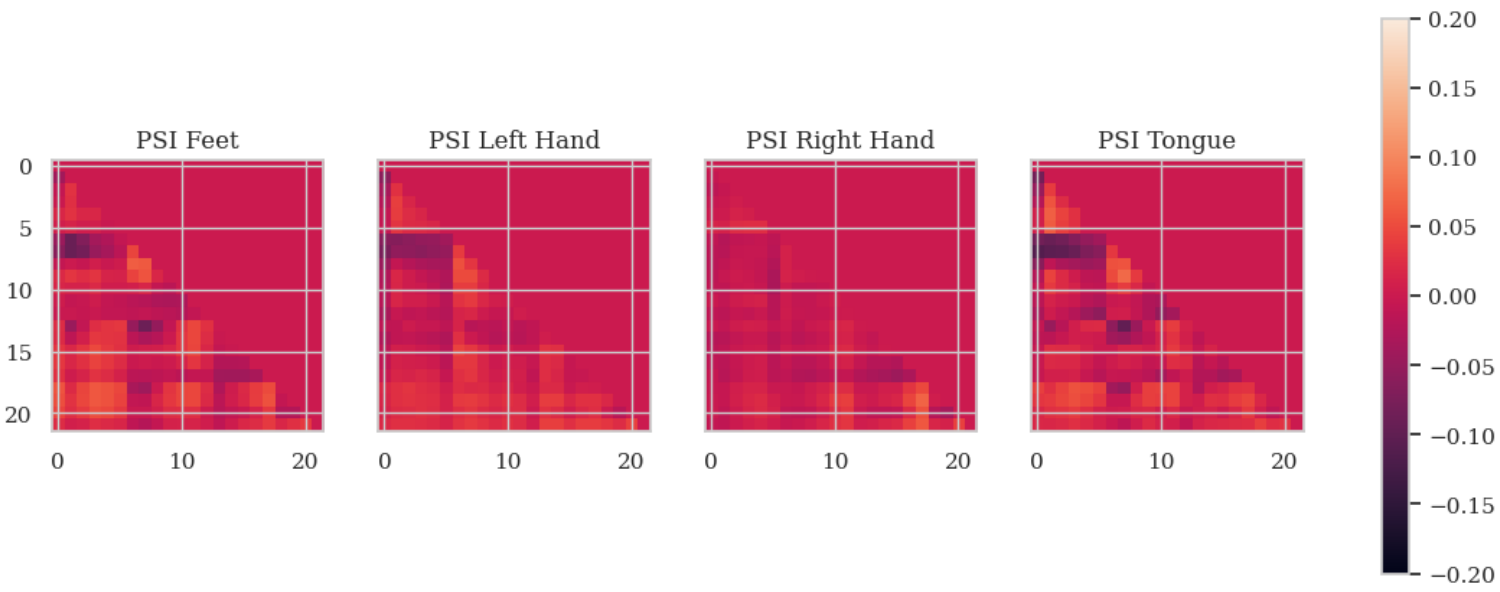

Figure 20: PSI Pairwise Adjacency Matrices

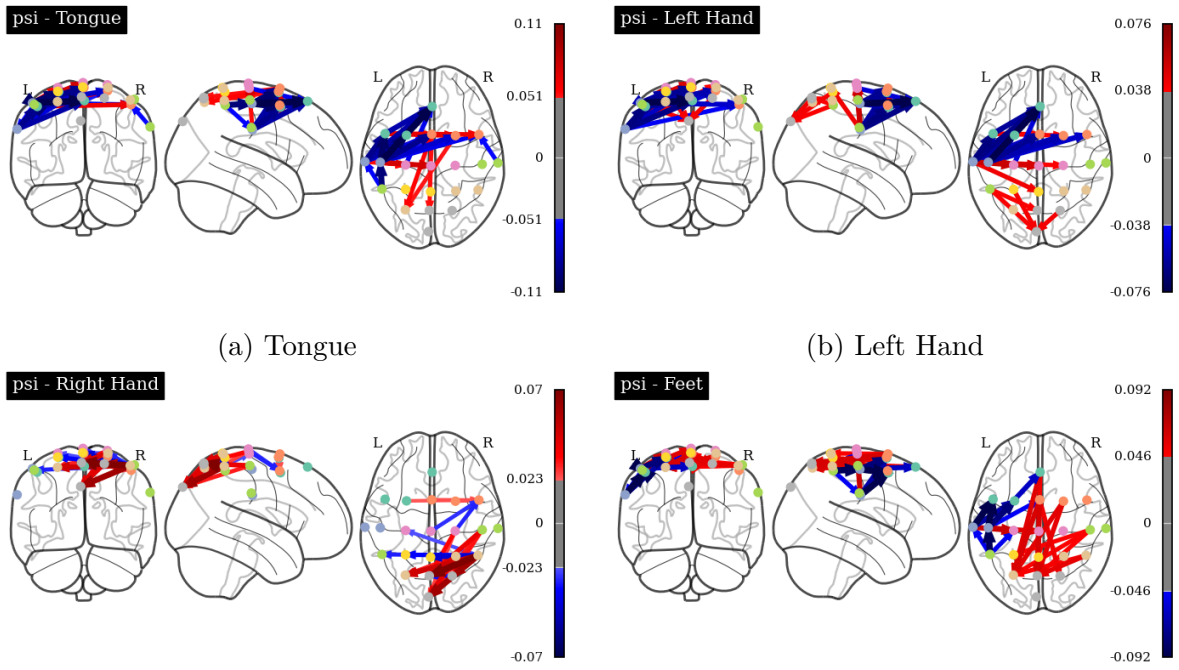

(a) Tongue

(b) Left Hand

(c) Right Hand

(d) Feet

Figure 21: Brain Connectivity Graphs using PSI

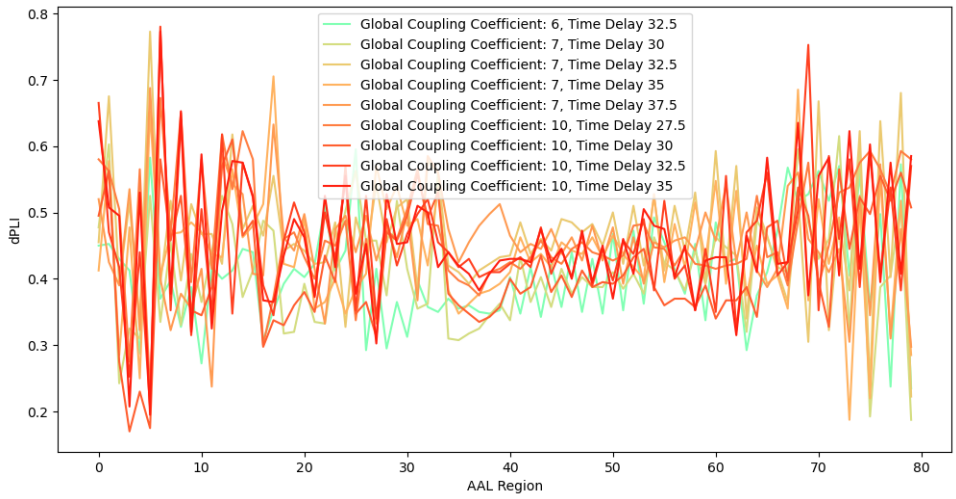

Figure 22: Parameter Search for WC-Model where $dPLI < 0.35$ or $dPLI > 0.65$

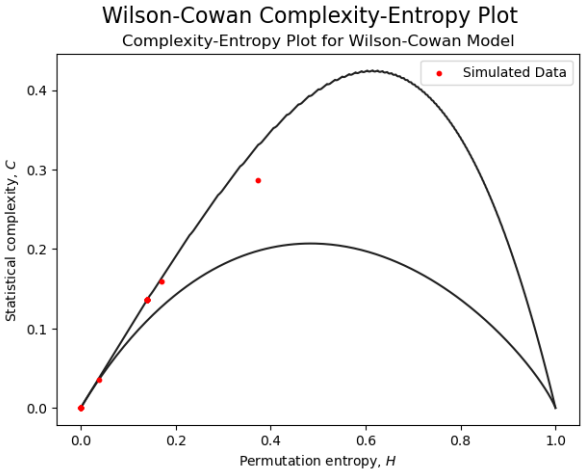

Figure 23: Complexity-Entropy Plot for WC Network